Atomic Spectroscopy

Article

Micro-XRF Mapping Study on the Taphonomy of A Jurassic Larval Salamander Fossil from Inner Mongolia of China

Yingyu Chen, [a,b] Xiaobo Li, [a,b,*] Fangfang Teng, [c] Jun Chen, [a,b] and Robert R. Reisz [a,d]

[a] Dinosaur Evolution Research Center, College of Earth Sciences, International Center of Future Science, Jilin University, Changchun 130012, P. R. China

[b] Biological Archaeology Laboratory of Jilin University, Changchun 130012, P. R. China

[c] Xinghai Paleontological Museum of Dalian, Dalian 116023, Liaoning, P. R. China

[d] Department of Biology, University of Toronto Mississauga, Mississauga, ON L5L 1C6, Canada

Received: *December 7, 2022;* ***Revised:*** *January 14, 2023.;* ***Accepted:*** *January 14, 2023.;* ***Available online:*** *January 24, 2023.*

DOI: 10.46770/AS.2022.246

ABSTRACT: Salamanders (Urodela) are members of a clade of extant amphibians whose fossil records extend far into the Mesozoic Era and have a classic body model of generalized tetrapods. The characteristic features of larval ontogenetic stages of early fossil salamanders can be used to better understand this group's origins and evolutionary history. This study used non-destructive micro-X-ray fluorescence (micro-XRF) imaging technology to explore the taxonomy and patterns of elemental concentrations of a Middle-Late Jurassic larval salamander fossil collected from northeastern China. P distribution mapping of the skeletal structure indicated that the fossil belongs to *Jeholotriton paradoxus*. Further analysis revealed that the skeleton is enriched with P, while the soft-tissue remains are enriched with Fe, Mn, Ga, and Cr. Ni and Zn in the trunk area come from the external environment. The Yanliao biota, to which the fossil belongs, contains many salamander fossils. Further XRF research will reveal more information about the ontogenesis and taphonomy of early salamanders.

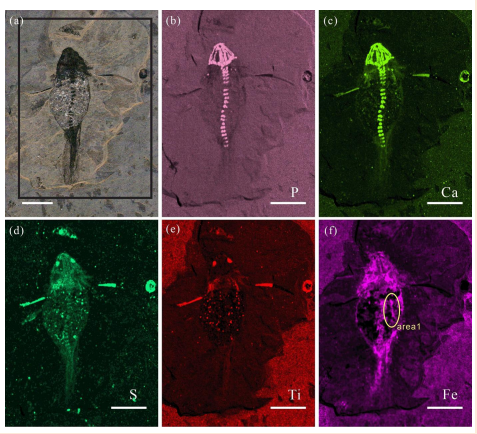

INTRODUCTION

The three major groups of living amphibians, Urodela, Anura, and Gymnophiona, belong to the lissamphibians. The late Mesozoic is the crucial period for their origin and radiation.[1-2] Compared with other groups of lissamphibians, salamanders (urodela) appear to have maintained a more conservative morphology. Consequently, the study of the early evolution of salamanders could shed light on the origin and evolution of lissamphibians. Generally, salamanders possess delicate bones and features that enable them to live in humid environments. These attributes make the preservation of their skeleton as fossils challenging. Thirty years ago, salamander fossils were rare, scattered, and fragmented.[3] However, by the end of the 20th century, thousands of well-preserved and exquisite salamander fossils at different stages of development were excavated and collected from the Mesozoic strata in the Yanliao region of northern China (including most areas of southeast Inner Mongolia, northern Hebei, and western Liaoning). These include taxa such as *Sinerpeton fengshanense*,[4] *Liaoxitriton zhongjiani*,[5] *Chunerpeton tianyiense*,[6] *Regalerpeton weichangense*,[7] and *Neimengtriton daohugouensis*.[8-9]

Most of these fossils retain articulated skeletons and soft-tissue impressions, which provide essential research data for understanding the early evolution of salamanders. The continuous discovery of related fossils in China and new fossils in North America and Europe,[7,10-11] revealed that there was only one kind of stem urodela *Triassurus* in the Middle-Late Triassic,[12] and other early salamanders mainly occurred in the Juro-Cretaceous strata. There are still many issues related to early salamanders' origins and phylogenetic relationships, partly because only a few fossil species and different characteristics have been selected for further

analyses. If poorly characterized taxa are excluded from evolutionary investigations or new fossils with more anatomical features are added, the results of phylogenetic analyses would change drastically,[13-15] emphasizing the need for more detailed studies.

To understand the details of the morphology and characteristics of salamanders, it is of great significance to study not only the adult forms of extinct taxa but also the juvenile and larval fossils. The juvenile and larval fossils possess unique features that will enhance our understanding of their ontogeny and evolution and provide information about habitats and paleoenvironmental conditions during fossil development.[2,16-17] For example, when comparing early salamander fossils to those of adults, the early salamander fossils were characterized by more diminutive size, partially ossified skeleton, and partially ossified skull elements.[6] Moreover, the preserved gill filaments, caudal fins, and other characteristics of larval fossils can reflect the living environment of larval salamanders (such as ponds or stream environments).[2,17] Furthermore, the immature skeleton and body size of larvae can provide details about the ontogeny of individual taxa and allow further studies of evolutionary branching models if different ontogenies are recovered in closely related taxa. For now, the early salamanders excavated from the Yanliao area in China have the largest number of preserved fossils in the world. More importantly, they are in an excellent state of preservation. However, these excellent research materials have mainly focused on the anatomy of the skeleton and the phylogeny of known taxa. Previous taphonomic studies of larval salamander fossils focused primarily on how to migrate to the burial site after death.[17] The burial process and mechanism of fossilization were not considered in any detail, and these can be generally related to the residues and later addition of some chemical elements in the fossils and the surrounding matrix.

In this study, a larval salamander fossil from the Daohugou Bed was scanned for chemical element distribution using emerging and non-destructive X-ray fluorescence (XRF) imaging to obtain valuable taphonomic information from the distribution pattern of related elements.[18-19] In the XRF imaging technology, the characteristic X-ray of various elements in the target sample is excited by using X-rays; qualitative and quantitative analyses are conducted after the identification of the elements. Recently, new XRF technologies, such as synchrotron rapid scanning X-ray fluorescence (SRS-XRF) and micro-X-ray fluorescence (micro-XRF), make it possible to conduct non-destructive analysis of large-scale (decimeter-scale) samples through area scanning under air or vacuum condition.[18,20] Non-destructive large-scale XRF imaging was first conducted to study the rare Late Jurassic Solnhofen *Archaeopteryx* fossil in Germany in 2010;[18] the results revealed the chemical composition of the fossil skeleton and feathers. Fossil feathers are not simple impressions as previously thought but are "chemical fossils," representing the residual elements of possible soft (and hard) tissues.[18] Since then, the XRF research of fossils has been expanded to Osteichthyes, reptiles, theropods, mammals, invertebrates, and plants.[21-24] This work represents the first use of non-destructive XRF imaging to study early salamander fossil; the results can elucidate the pattern of elemental distribution and allow the reconstruction of the taphonomy of Jurassic larval salamander fossil in the Yanliao area. Moreover, the data disclosed herein can guide the research of the fossilization process of other well-preserved fossils (such as adult salamanders and other tetrapods) in this area.

MATERIALS AND METHODS

Early larval salamander fossil. The fossil specimen studied in this paper was collected from the Middle-Upper Jurassic Daohugou bed (the Haifanggou Formation) in the Daohugou locality, Ningcheng County, Inner Mongolia, China.[25-26] The lithology of the matrix around the fossil is grayish shale. The fossil was stored at the Dinosaur Evolution Research Center of Jilin University (Jilin, China), and the specimen number is DERC-Z0018. The Daohugou biota is part of the early assemblage of the Yanliao biota in China. It has preserved fossils of various plants, invertebrates, and vertebrates, which are highly important to studying insects, birds, and early mammals.[26-27] Three species of early salamanders have been found and reported in the Daohugou area of the Yanliao biota: metamorphosed *Neimengtriton daohugouensis*, neotenic *Jeholotriton paradoxus*,[3,28-29] and *Chunerpeton tianyiense*. The characteristics of some juvenile and adult skeletons of these three salamanders have been reported in detail and will be used for a comparative discussion in this study. We also selected the juvenile specimen (RCPS VL2002) of *Jeholotriton paradoxus* (the tail is missing, with a total length of more than 80 mm) and the adult specimen (JLUM-H-Al170701a) of *Chunerpeton tianyiense* (complete articulated skeleton, with a total length of approximately 180 mm) as comparative materials.

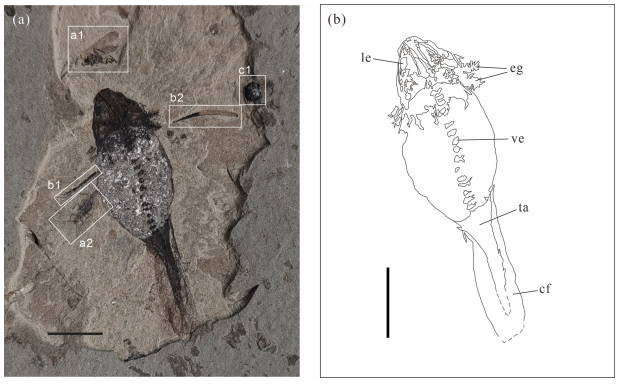

Fig. 1 (a) Optical image of the larval salamander DERC-Z0018. (b) Line drawing of the specimen: a1 and a2 are insect fossils; b1 and b2 are residues similar to stems; c1 area is the remains of unknown black mass. The scale is 10 mm. cf, caudal fin; eg, external gills; le, lens; ta, tail; ve, vertebra.

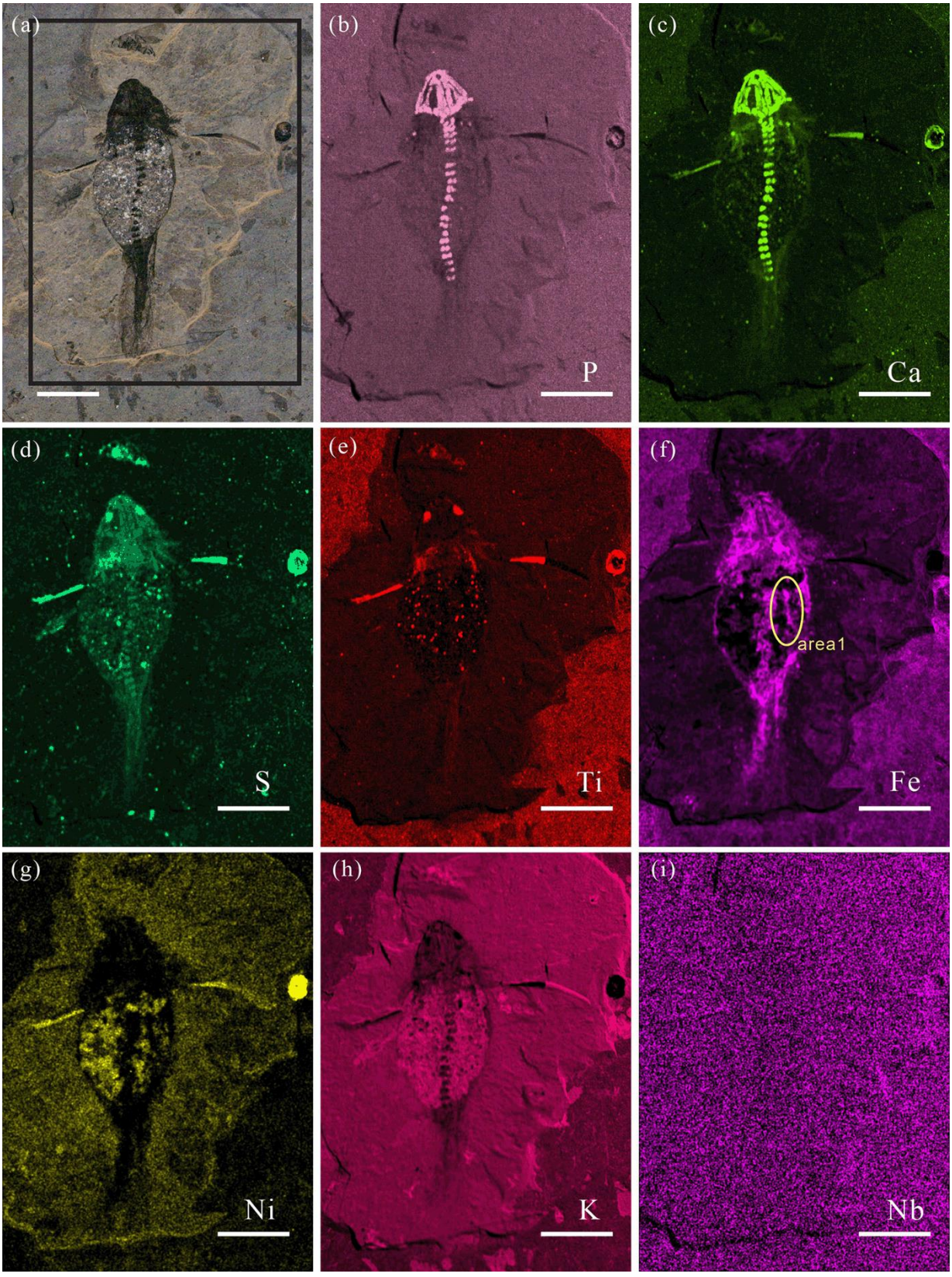

Fig. 2 (a) Black box shows the actual scanning area of DERC-Z0018. (b)–(i) Micro-XRF false color element distribution maps. Each map corresponds to the following elements: (b) P, (c) Ca, (d) S, (e) Ti, (f) Fe, (g) Ni, (h) K, and (i) Nb. The brighter the color, the more enriched the element. The yellow oval area (area 1) shows the specific enrichment of Fe (f), respectively. The scale is 10 mm.

There was no trace of limbs near the trunk of the salamander, and the caudal fin was expanded, indicating that the salamander was in the larval stage. The length from the snout to the tail was approximately 45.5 mm. This young salamander shows dark black soft-tissue residues on its head and rear tail, except that its trunk is gray and mixed with white crystalline minerals. The vertebrae at the trunk are also black, indicating that the skeleton is mainly preserved as black bone, including residual cranial bones. In addition to the main salamander fossil, insect fossils (Figs. 1a1and 1a2) were preserved on the front side of the head and left side of the trunk. There were residues similar to plant stems (Figs. 1b1and 1b2) on the external gills, and an unknown oval black mass remained on the side of the stems (Fig. 1c1). The elemental distributions of these other fossils on the slab provide comparisons and references for studying the salamander. To facilitate the identification of these fossils, an area code was used to indicate the fossils themselves.

Institutional abbreviations: DERC, Dinosaur Evolution Research Center, Jilin University; RCPS, Research Center of Paleontology and Stratigraphy, Jilin University.

Micro-XRF mapping. The specimen was analyzed using an M4 TORNADO^{PLUS} micro-XRF spectrometer (Bruker Nano GmbH, Berlin, Germany) at the Key Laboratory of Earth and Planetary Physics, Institute of Geology and Geophysics, Chinese Academy of Sciences (Beijing, China). The size of the motorized servo X-Y-Z stage was 330 mm × 170 mm (W × D), and the movable range was 200 mm × 160 mm × 120 mm (W × D × H). It can operate under atmospheric/vacuum conditions and can conduct qualitative and semi-quantitative analysis of elements through area scanning. Compared with the M4 TORNADO spectrometer before upgrading, this instrument is equipped with two large-area silicon drift detectors (SDD) with super-light element windows, which can detect and analyze light element carbon, and an innovative aperture management system (AMS) is added, which can perform ultra-depth of field processing on samples with uneven surfaces. It is equipped with a high-throughput pulse processor to improve test efficiency and a sample stage that can be quickly replaced. These updates enable faster data acquisition to achieve higher accuracy. This experiment ran at the maximum energy setting (50 kV, 600 μA), under vacuum (2.4 mbar), and did not use filters. The excitation light source was a high-intensity X-ray tube (Rh target) equipped with polycapillary focusing optics, and the spot size was 20 μm. The resolution (pixel size) was set to 20 μm. The data acquisition speed was 8 ms/pixel, the selected scanning area was a rectangle (2165 × 2915 pixels), and the total scanning time was 16 h 17 min. After data collection, the characterization software provided by Bruker Micro Analytics was used to analyze and generate the sample's elemental content data, element distribution maps, and heat maps (Fig. 2, Figs. S1, and S2). The single-element distribution map is a monochromatic false-color image. Color has no practical significance and is used only to display the presence and concentration of elements. Different element distribution maps can be displayed by superimposition. The heat map uses a series of colors to show the enrichment and distribution of a single element more clearly, which cannot be superimposed.

RESULTS

Identification of the spectrogram. The spectrogram of the scanning area obtained by XRF showed that the scanning area of the specimen was mainly composed of O, Si, Al, K, Fe, Na, Ca, Mg, Ti, Mn, S, and other elements (Fig. 3). These elements are shown by the peaks at the corresponding energy of their characteristic X-ray. In the spectrogram, in order to display the existence of all Kα related energy peaks of the elements in the study specimen, the main scale of the y-axis increases exponentially at a rate of 10. Because the value span is too large, the signal of some elements (such as Ni, Zn, and Ga) appears relatively weak. Actually, the peaks of these elements are obvious, so it is meaningful to identify these elements and study the relevant distribution maps. It is worth noting that the characteristic peaks of different elements may overlap, such as V-Kα and Ti-Kβ, or Co-Kα and Fe-Kβ. It is necessary to determine the element indicated by the peak, because the nonexistent element and its distribution map have no research significance. Through determination, interference elements such as Cl, V, and Co are excluded, laying a

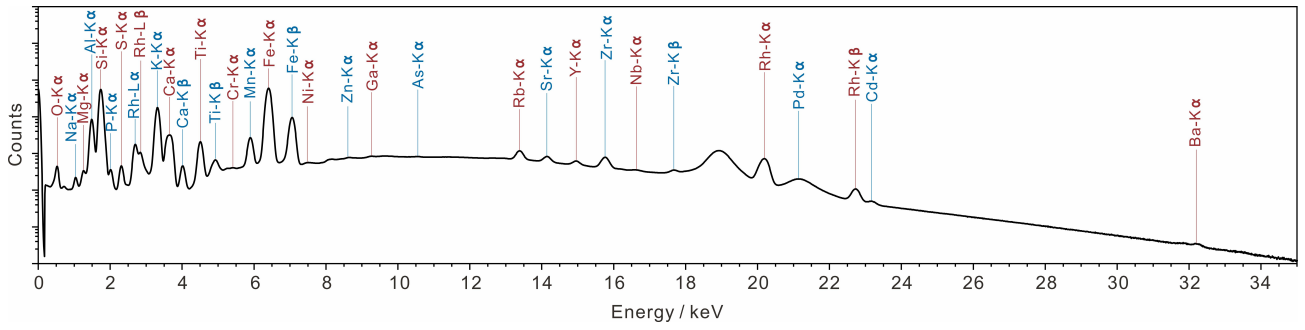

Fig. 3 Spectrogram of the micro-XRF scanning area of DERC-Z0018.

good foundation for in-depth analysis of two-dimensional element distribution map.

Element distribution patterns revealed by element distribution maps and heat maps. The information obtained from the spectrogram and data is limited, and only overall details on the scanning area (including the matrix and fossils) are available. In addition, the element distribution map shows the state and distribution of element enrichment, which is of great significance in distinguishing and comparing matrix and fossils. Through observation and combined with a single-element heat map, the element distribution map mainly shows three modes (excluding the analysis of secondary minerals scattered in the body of the salamander):

The first is the elements that significantly correlate with the fossils, such as Ca, Cr, Fe, Ga, Mn, Ni, P, S, Ti, and Zn (Fig. 2, Figs. S1 and S2). P only showed a significant correlation with the salamander skeleton in relation to the matrix. Ca and S are related to the skeleton and show different degrees of correlation with other biological tissues (soft/hard tissues), including other nearby fossils. Ca showed the highest concentration in the salamander skeleton and c1, followed by b1 and b2, and was also concentrated in the salamander head, external gills, body contour, and some areas of a1. S is most concentrated at b1, b2, and c1, followed by a1 and the salamander lens. The concentration of S in the head remains, the skeleton of the salamander, and a2 is higher than that in the trunk and tail of the salamander. Ti is significantly related to the lens, and external gills of the salamander, b1, b2, and c1, and are also associated with a1. The salamander's dark remains were mainly enriched in Fe, Mn, Ga, and Cr. Fe and Mn showed a stronger contrast than Ga and Cr in relation to the matrix. These four elements may be related to the late mineralization of fossil remains to a large extent. Interestingly, these elements showed lower concentrations at b1, b2, and c1 than in the matrix. The Ni and Zn enrichment areas in the salamander were opposite to elements such as Fe and Mn. Ni and Zn showed higher concentrations in b1 and b2 than in the matrix and were most enriched in c1.

The second is the elements that are mainly enriched in the matrix and rarely contained in the salamander, including Al, K, and Si (Fig. 2, Figs. S1 and S2). K showed higher concentrations in a1, a2, and salamander torso mineralization areas than in the matrix. a1 and a2 showed clear morphological outlines in the K-distribution map.

The third is the uniform distribution of elements in the study specimen, including Ba, Cd, Nb, Sr, and other elements (Fig. 2, Fig. S1 and S2). Except for the heaviest Ba distribution map, the depth of field cannot be seen. In contrast, the other element distribution maps show the undulation of the surface because the specimen is uneven.

In addition to the above distribution patterns, some elements were sporadically enriched in the distribution maps. For example, Y only showed apparent enrichment in the salamander head's left bone and nasal area and only scattered and dotted enrichment in other parts of the skeleton (Fig. S1 and S2). Y shows uneven mineralization in skeleton, and the different enrichment states of these elements above show the heterogeneous and complex mineralization processes that the fossils have to undergo in the taphonomy process.

COMPARISON AND DISCUSSION

Various fossils of the specimen. A variety of fossils was distributed on the slab's surface containing the urodela. Except for the salamander, Figs. 1a1 and 1a2 can be interpreted as the remains of arthropods. However, b1 and b2 have no complex biological structures, and there are apparent differences between them and other animal tissues on the block. At the same time, they have elemental distribution patterns similar to those the Eocene plant fossils *Platanus wyomingensis* (in relation to the matrix, they are more enriched in Zn and Ni and do not contain Mn).[22] Therefore, it can be inferred that b1 and b2 are the stems of plants. The element distribution pattern of c1 was very similar to that of b1 and b2. In most cases, the element concentration of c1 is higher than that in the b1, and b2 regions, so c1 may be the seeds or other parts of the plants with a larger volume.

Under the same burial environment, salamander, arthropod (a1, a2), and plant fossils (b1, b2, c1) showed different element enrichment states compared with the matrix, and different taphonomy results were established because of the various structures and characteristics of the fossils. The black remains (soft tissues) of salamander are mainly enriched in Fe, Mn, Ga, and Cr, the skeleton is enriched in P, the whole body is enriched in Ca, and S. Ti is mainly enriched in the eye lens, external gills, and other areas. There are also elements such as Y in local areas. Arthropods are rich in K and S, as well as Ti and Ca in local areas. Plant fossils were rich in Ca, S, Zn, Ni, Ti, and other elements. The striking difference between the salamander and the other fossils is that the elements are mainly concentrated in the black areas; thus, the elements are only concentrated in the skeletal region of the salamander. Salamander and plant fossils have more abundant element enrichment than arthropods, which shows that more information related to individuals and mineralization has been left after burial.

Information of larval salamander revealed by element distribution maps. Overall, the related elements of the salamander showed various enrichment states. Elements in different distribution states revealed additional information about

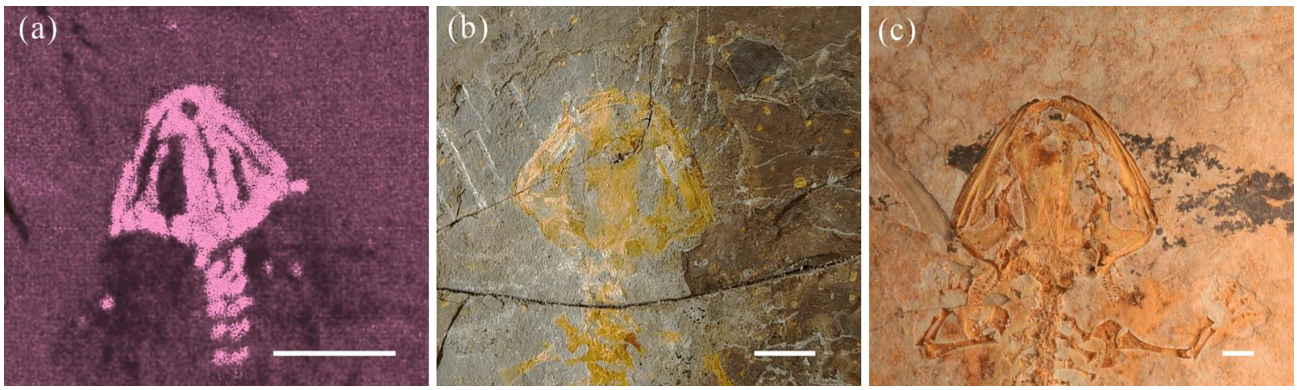

Fig. 4 Comparison of skull skeleton of salamander fossils. (a) Distribution map of P in DERC-Z0018 enlarged view of skull region. (b) optical image of the juvenile *Jeholotriton paradoxus* (RCPS VL2002). (c) optical image of adult *Chunerpeton tianyiense* (JLUM-H-Al170701a). The scale is 5 mm.

the larval salamander, including ontogeny and mineralization.

Compared with Ca and S, the elemental distribution map of P shows a clearer view of the skeletal structure of the salamander (Fig. 2 and Fig. S1). The P distribution map showed that the skull bones were not fully developed or sutured. One fenestra appeared between the anterior nasals, indicating that some nasals were undeveloped, and the pterygoid was long and extended medially. At the intersection of the external gills, there were small bones, which may be related to the supporting role of the gills. The vertebrae are mainly cervical vertebrae, trunk vertebrae, and sacral vertebrae, which are not entirely developed; most of the caudal vertebrae are probably still in the cartilaginous state have not yet been fully ossified. Limb bones were not observed in the three element distribution maps, and there were no specific residues of elements in the relative positions of the other element distribution maps, indicating that the larva is at an early stage of development and its forelimbs have not been ossified. In the past, three species of salamander fossils were excavated from Jurassic strata in this area (the Yanliao area). The juvenile specimen (IVPP V18085) of *Chunerpeton tianyiense* with a total length of approximately 35 mm shows an apparent forelimb skeleton,[16] while the fossil studied in this paper is about 45.5 mm long without a limb skeleton, so the growth and development stages appear to vary in these two taxa. The adult specimen (PKUP V0515) of *Neimengtriton daohugouensis* has a broad and round snout, and the palatal process of pterygoids expands bilaterally.[9] However, the skeleton studied in this paper does not show this feature. The length of the IVPP V14195B, a juvenile specimen of *Jeholotriton paradoxus*, was 96 mm, and its snout was narrower than that of *Neimengtriton*. The front end of the preserved left pterygoid is slender and extends inward.[16] These two features are similar to our specimen (Fig. 4a), and related adult fossils (such as IVPP V11944B) also inherit and develop these features.[3] At the same time, the reference specimen (RCPS VL2002) of *Jeholotriton* also shows cranial skeletal characteristics similar to our research specimen (Fig. 4b). The distinct medial process of the pterygoid in the reference specimen (JLUM-H-Al170701a) of *Chunerpeton* indicates that the fossil was quite different from research specimen in current paper (Fig. 4c). Therefore, the research specimen can be identified with some confidence as the larval stage of *Jeholotriton paradoxus*.

P appears to be enriched only in the skeleton, showing that the skeleton was preserved as carbon impressions and contains apatite components in the skeleton of general vertebrate fossils. The distribution areas of Fe, Mn, Ga, and Cr, mainly enriched in the black remains, show that the organic matter of the fossil has diffused to a certain extent in the process of decomposition and fossilization, resulting in the scattered retention of elements, which are generally distributed along the fossil area. The enrichment of Fe on the right side of the vertebrae along the trunk (Fig. 3f, area1) may indicate the location of the dorsal fin. Ni and Zn, opposite to Fe distribution, were mainly distributed in the trunk. The interior of the trunk is soft tissue, which is the first area to be decomposed and replaced compared with hard tissues such as skeleton. The enrichment of Ni and Zn indicates the introduction of these elements in the later taphonomy process. These elements are not related to biomineralization, but only to inorganic minerals related to burial. Ca and S throughout the salamander have different enrichment concentrations in various parts, of which S shows higher concentrations than the matrix in all fossils of this specimen, which strongly indicates that S is related to organic remains.

CONCLUSION

The elemental distribution maps of micro-XRF revealed valuable information about the ontogeny and taphonomy of the Jurassic laval specimen of *Jeholotriton paradoxus* in Ningcheng, Inner Mongolia. We conclude that because of the differences in the general composition of the skeleton, soft tissues, and lens, they are

replaced by different elements during burial. The distribution of P is mainly correlated with well-developed areas of the skeleton, which indicates that the salamander was at a larval stage where it did not have well-developed limbs and complete caudal vertebrae. The skeletal structure of the fossil was more clearly observable through the P distribution map, allowing its identification as *Jeholotriton*. The distribution of Ca and S observed in this study appears to be controlled by the overall morphology of the salamander. Still, the concentration was uneven, revealing the finer structures of this larval salamander (Ca) as well as indicating the preservation of organic remains (S). Ti is dominant in the ocular lens. Ni and Zn enriched in trunk are introduced during burial.

This study is the first to apply non-destructive XRF-mapping technology to the study of an early salamander fossil and reveal the taphonomic characteristics and mineralization of a larval salamander. It is worth mentioning that many salamander fossils have been unearthed in the fossil locality. These fossils are larvae, juveniles, and adults. The specimens were preserved on flat plates. The skeleton was maintained very well, and soft tissues were mostly preserved, which is suitable for future XRF studies focusing on preservation patterns, ontogeny, and overall taphonomy of such fossils.

ASSOCIATED CONTENT

The supporting information (Figs. S1−S2) is available at www.at-spectrosc.com/as/home

AUTHOR INFORMATION

Xiaobo Li received his BSc in 2004 and PhD in 2011 from the Jilin University. He is an associate professor of paleontology and stratigraphy in the College of Earth Sciences, Jilin University. His major research interests are vertebrate evolution and paleoecology, stratigraphy and sedimentology, paleogeography and basin analysis. Recently, he used some advanced techniques and methods to explore the formation of exceptionally preserved fossils.

Corresponding Author

*X. B. Li

Email address: lixiaobo@jlu.edu.cn

Notes

The authors declare no competing financial interest.

ACKNOWLEDGMENTS

This work was supported financially by the NSFC Basic Science Center Project (42288201) and the National Rock, Mineral and Fossil Specimen Resource Bank Project (3D5201540506). We thank Prof. Jinhua Li for supporting the laboratory works in his lab and inviting us to submit current paper to Atomic Spectroscopy; thanks to Prof. Wenhao Wu for providing a specimen RCPS VL2002 in this research, as well as Kelei Zhu and Yan Liu, who have helped us in the XRF experiment. We sincerely thank the review experts for their suggestions on the revision of this paper.

REFERENCES

1. R. Carroll, *Nature*, 2001, **410**, 534–536. https://doi.org/10.1038/35069181
2. K. Q. Gao, J. Y. Chen, and J. Jia, *Can. J. Earth Sci.*, 2013, **50**, 255–267. https://doi.org/10.1139/e2012-039
3. Y. Wang, *Vert. PalAsiat.*, 2000, **38**, 100–103 and 161–164. https://doi.org/10.19615/j.cnki.1000-3118.2000.02.003
4. K. Q. Gao and N. H. Shubin, *Nature*, 2001, **410**, 574–577. https://doi.org/10.1038/35069051
5. Z. M. Dong and Y. Wang, *Vert. PalAsiat.*, 1998, **36**, 159–172. https://doi.org/10.19615/j.cnki.1000-3118.1998.02.006
6. K. Q. Gao and N. H. Shubin, *Nature*, 2003, **422**, 424–428. https://doi.org/10.1038/nature01491
7. Y. F. Rong, *Vert. PalAsiat.*, 2018, **56**, 121–136. https://doi.org/10.19615/j.cnki.1000-3118.170627
8. Y. Wang, *Chin. Sci. Bull.*, 2004, **49**, 814–815. https://kns.cnki.net/kcms/detail/detail.aspx?dbcode=CJFD&dbname=CJFD2004&filename=KXTB200408018&uniplatform=NZKPT&v=CFRpcX9kAPkCJ-MiMLDccSEEkDWMPdd6OU9kXTFdeUFcIpY4TR4XecFAYNPJCiuI
9. J. Jia, J. S. Anderson, and K. Q. Gao, *iScience*, 2021, **24**, 102744. https://doi.org/10.1016/j.isci.2021.102744
10. P. P. Skutschas, V. V. Kolchanov, and A. H. Schwermann, *Cretac. Res.*, 2020, **116**, 104606. https://doi.org/10.1016/j.cretres.2020.104606
11. J. D. Gardner, *Acta Palaeontol. Pol.*, 2022, **67**, 35–50. https://doi.org/10.4202/app.00926.2021
12. R. R. Schoch, R. Werneburg, and S. Voigt, *Proc. Natl. Acad. Sci. USA*, 2020, **117**, 11584–11588. https://doi.org/10.1073/pnas.2001424117
13. Y. F. Rong, D. Vasilyan, L. P. Dong, and Y. Wang, *Palaeoworld*, 2021, **30**, 708–723. https://doi.org/10.1016/ j.palwor.2020.12.001
14. M. E. H. Jones, R. B. J. Benson, P. Skutschas, L. Hill, E. Panciroli, A. D. Schmitt, S. A. Walsh, and S. E. Evans, *Proc. Natl. Acad. Sci. USA*, 2022, **119**, e2114100119. https://doi.org/10.1073/pnas.2114100119
15. J. Jia, G. Z. Li, and K. Q. Gao, *eLife*, 2022, **11**, e76864. https://doi.org/10.7554/eLife.76864
16. L. P. Dong, D. Y. Huang, and Y. Wang, *Chin. Sci. Bull.*, 2012, **57**, 72–76. https://doi.org/10.1007/s11434-011-4729-z

17. J. Jia and K. Q. Gao, *PeerJ*, 2016, **4**, e2499. https://doi.org/10.7717/peerj.2499
18. U. Bergmann, R. W. Morton, P. L. Manning, W. I. Sellers, S. Farrar, K. G. Huntley, R. A. Wogelius, and P. Larson, *Proc. Natl. Acad. Sci. USA*, 2010, **107**, 9060–9065. https://doi.org/10.1073/pnas.1001569107
19. R. A. Wogelius, P. L. Manning, H. E. Barden, N. P. Edwards, S. M. Webb, W. I. Sellers, K. G. Taylor, P. L. Larson, P. Dodson, H. You, L. Da-qing, and U. Bergmann, *Science*, 2011, **333**, 1622–1626. https://doi.org/10.1126/science.1205748
20. J. H. Li, R. Pei, F. F. Teng, H. Qiu, R. Tagle, Q. Q. Yan, Q. Wang, X. L. Chu, and X. Xu, *Atom. Spectrosc.*, 2021, **42**, 1–11. https://doi.org/10.46770/AS.2021.01.001
21. M. J. Pushie, B. R. Pratt, T. C. Macdonald, G. N. George, and I. J. Pickering, *Palaios*, 2014, **29**, 512–524. https://doi.org/10.2110/palo.2014.073
22. N. P. Edwards, P. L. Manning, U. Bergmann, P. L. Larson, B. E. van Dongen, W. I. Sellers, S. M. Webb, D. Sokaras, R. Alonso-Mori, K. Ignatyev, H. E. Barden, A. van Veelen, J. Anné, V. M. Egerton, and R. A. Wogelius, *Metallomics*, 2014, **6**, 774–782. https://doi.org/10.1039/C3MT00242J
23. P. Gueriau and L. Bertrand, *Microsc. Today*, 2015, **23**, 20–25. https://doi.org/10.1017/S1551929515000024
24. P. L. Manning, N. P. Edwards, U. Bergmann, J. Anné, W. I. Sellers, A. van Veelen, D. Sokaras, V. M. Egerton, R. Alonso-Mori, K. Ignatyev, B. E. van Dongen, K. Wakamatsu, S. Ito, F. Knoll, and R. A. Wogelius, *Nat. Commun.*, 2019, **10**, 2250. https://doi.org/10.1038/s41467-019-10087-2
25. C. Sullivan, Y. Wang, D. W. E. Hone, Y. Q. Wang, X. Xu, F. C. Zhang, *J. Vertebr. Paleontol.*, 2014, 34, 243–280. https://doi.org/10.1080/02724634.2013.787316
26. D. Y. Huang, *Acta Palaeontol. Sin.*, 2015, **54**, 501–546. https://doi.org/10.19800/j.cnki.aps.2015.04.008
27. F. Liu, R. Wu, and F. L. Han, *Acta Palaeontol. Sin.*, 2022, **61**, 88–106. https://doi.org/10.19800/j.cnki.aps.2020027
28. Y. Wang and C. S. Rose, *J. Vertebr. Paleontol.*, 2005, **25**, 523–532. https://doi.org/10.1671/0272-4634(2005)025[0523:JPACFT]2.0.CO;2
29. R. Carroll and A. Zheng, *Zool. J. Linn. Soc.*, 2012, **164**, 659–668. https://doi.org/10.1111/j.1096-3642.2011.00777.x